AGU PUBLICATIONS

Water Resources Research

RESEARCH ARTICLE
10.1002/2014WR015365

Spatiotemporal flood sensitivity to annual precipitation: Evidence for landscape-climate coevolution

Rui A. P. Perdigão[1] and Günter Blöschl[1]

[1]Institute of Hydraulic Engineering and Water Resources Management, Vienna University of Technology, Vienna, Austria

Key Points:
- Spatial and temporal sensitivities of floods to precipitation can differ
- Symmetry breaks relate to landscape-climate coevolution
- Simple dynamical model of coevolution supports statistical results

Correspondence to:
R. A. P. Perdigão,
perdigao@hydro.tuwien.ac.at

Citation:
Perdigão, R. A. P., and G. Blöschl (2014), Spatiotemporal flood sensitivity to annual precipitation: Evidence for landscape-climate coevolution, *Water Resour. Res.*, *50*, 5492–5509, doi:10.1002/2014WR015365.

Received 27 JAN 2014
Accepted 16 JUN 2014
Accepted article online 18 JUN 2014
Published online 7 JUL 2014

Abstract This study investigates the sensitivity of floods to annual precipitation in space and time and evaluates quantitative signs of landscape-climate coevolution. For that purpose, a spatiotemporal sensitivity analysis is performed at regional scale using data from 804 catchments in Austria from 1976 to 2008. Results show that flood peaks are more responsive to spatial (regional) than to temporal (decadal) variability. Space-wise a 10% increase in precipitation leads to a 23% increase in flood peaks in Austria, whereas time-wise a 10% increase in precipitation leads to an increase of just 6% in flood peaks. Catchments from dry lowlands and high wetlands exhibit similarity between the spatial and temporal sensitivities (spatiotemporal symmetry) and low landscape-climate codependence. This suggests that such regions are not coevolving significantly. However, intermediate regions show differences between those sensitivities (symmetry breaks) and higher landscape-climate codependence, suggesting undergoing coevolution. A new coevolution index is then proposed relating spatiotemporal symmetry with relative characteristic celerities. The descriptive assessment of coevolution is complemented by a simple dynamical model of landscape-climate coevolution, in which landform evolution processes take place at the millennial scale (slow dynamics), and climate adjusts in years to decades (fast dynamics). Coevolution is expressed by the interplay between slow and fast dynamics, represented, respectively, by spatial and temporal characteristics. The model captures key features of the joint landscape-climate distribution, supporting the descriptive assessment. This paper ultimately brings to light that coevolution needs to be taken into account through characteristic celerities in space-time trading of regional hydrology.

1. Introduction

Recent major river floods around the world have raised concerns that floods may have increased due to changes in their controls. As river floods are mainly driven by precipitation and snowmelt, any changes in precipitation amount will cause changes in the flood magnitudes. However, the degree of dependence is not yet clear.

Precipitation causes floods at a number of time scales [*Merz et al.*, 2012]. The most obvious effect is at the event scale. If event runoff coefficients remain the same, an increase in event precipitation translates proportionally into an increase in flood volume and consequently peak runoff [*Rogger et al.*, 2012]. Increasing event precipitation tends to accelerate response times, which will cause a further increase the flood peaks. However, there are more indirect effects at longer time scales [*Sivapalan et al.*, 2005]. Seasonal and annual precipitation will affect the antecedent catchment soil moisture of individual events, which will affect the flood magnitudes. Additional complexities may be involved if the vegetation and soils adjust to decadal and centennial changes in precipitation, not to mention other factors such as land use changes. Relating event precipitation to event runoff may therefore not fully capture the sensitivities of flood runoff to precipitation across time scales. Decadal oscillations of extreme precipitation are often highly correlated with those of longer-term averages [*Ntegeka and Willems*, 2008] through oscillations in weather patterns [*Knox*, 2000]. Because of this, the sensitivity of floods to precipitation is of particular interest.

As an alternative to long-term studies, it has been suggested to examine the spatial variability of the variable of interest, say annual maximum flow, in order to infer its sensitivity. This approach has been termed space-for-time substitution in ecology [*Pickett*, 1989] and geomorphology [*Abrahams*, 1972] and is based on Jenny's chronosequence concept [*Jenny*, 1941]. The idea is to analyze how two or more variables covary in space, in order to understand their connection in time. In essence, this is also the basis of regional flood frequency analysis where space is traded for time [*Hosking and Wallis*, 1997; *Peel and Blöschl*, 2011]. In the

present context, this implies that, instead of analyzing temporal sensitivity of floods to precipitation for a single catchment, one analyses different catchments with different climate/hydrological characteristics across gradients, assuming that the spatial changes in precipitation, runoff generation characteristics, runoff regime and flood occurrence, can be mapped to their temporal covariability.

Note, however, that while relatable and thus tradable, spatial and temporal statistics have to be exercised with care. In fact, spatial features do not change instantly and may evolve differently in time depending on local or regional conditions. For instance, land use changes may take several years to be reflected on corresponding soil properties [*Runyan et al*., 2012]. Another example comes from landscape-climate coevolution, which brings out a close linkage between the precipitation regime and the soils and landform, themselves important controls of floods at the event scale [*Gaál et al*., 2012; *Blöschl et al*., 2013; *Jefferson et al*., 2010]. Despite such interconnections, landscape-climate feedbacks are not synchronous. Rather, they take place at different time scales [*Skøien et al*., 2003], with climate readjusting under its controls in a matter of decades whereas landscape responses may take millennia to unfold [*Harvey*, 2002].

The relation between spatial and temporal statistics can be evaluated by comparing spatial with temporal sensitivity of floods to precipitation. The reasons underneath the sensitivity diagnosis can then be assessed in the light of underlying spatiotemporal mechanisms such as the coevolution between landscape and climate.

The aim of the present study is therefore to understand the sensitivity of floods to mean annual precipitation in space and time, evaluate its space-time symmetry and quantitative signs of landscape-climate coevolution. The interest is in particular on the process interpretation of this sensitivity in space and time, its relation to coevolution and ultimately a better understanding of the coevolution process itself. The analyses are based on a data set of annual maximum floods in 804 catchments in Austria with a record length of 33 years. For that purpose, a spatiotemporal analysis is conducted in section 2, followed by an evaluation of space-time symmetry, eventual symmetry breakups, and underlying mechanisms at play, namely coevolution between landscape and climate (section 3). Coevolution is further addressed quantitatively by discussing processes and feedbacks, leading to the introduction of a simple dynamical model of landscape-climate coevolution (section 4). The practical analysis is conducted in section 5, presenting results on spatiotemporal sensitivity, symmetry measure, and signs of coevolution, along with the comparison between the model introduced in section 4 and the observational data sets.

2. Spatiotemporal Analysis Method

2.1. Study Region and Its Hydroclimatic Properties

Addressing the joint spatiotemporal variability at regional and decadal scales requires significant hydrological variability across a sufficiently dense spatiotemporal data network. Austria qualifies for that purpose due to its strongly heterogeneous landscape, shaping a diversity of weather patterns and catchment characteristics as captured by a dense data network. In this study we consider the five hydroclimatic regions in Austria defined by *Merz and Blöschl* [2009] along with the country as a whole: (1) "Alpine Region," corresponding to the westernmost mountainous areas located in the Alps; (2) "Southern Alpine Region," covering East Tirolean alpine areas, catchments along the river Gail in the southernmost part of the country, and the lower alpine areas to the southeast; (3) "Northern Alpine Region," on the northernmost central Alps; (4) "Northern Lowlands," rather flat areas in the northwest of Austria; (5) "Eastern Lowlands," to the East and Northeast. In terms of dominant processes in runoff generation, snow and glacier melt take the lead in regions 1 and the northern parts of region 2, though in the latter weather storm systems coming from the Mediterranean play a significant role. As for region 3, the dominant controls come from orographic precipitation due to the alpine barrier posed to northwesterly atmospheric flows. This region is the rainiest of the five considered. Regions 4 and 5 exhibit predominant weather-related controls, with a prevalent synoptic rather than orographic nature. Precipitation in these regions is lower than in the others, with region 5 being the driest of all five. This is due to its continental climate with dry and warm summers and snow-poor cold winters.

2.2. Data Set and Processing Framework

We analyze time series of annual catchment precipitation and maximum annual flood peaks for each of 804 catchments geographically distributed throughout Austria over 33 years, namely from 1976 till 2008. These series for precipitation and flood peaks are then grouped in data matrices $P_{s,t}$ and $\mathcal{Q}^p_{s,t}$, respectively, where

Table 1. Mean and Standard Deviation of Specific Flood Peaks[a]

	Hydroclimatic Region					
		Region 1	Region 2	Region 3	Region 4	Region 5
Moments ($m^{1.5}s^{-1}$)	All Austria	C. Alps	S. Alps	N. Alps	N. Lowlands	E. Lowlands
$\mu(Q^p)$	0.7031	1.0304	0.5495	1.1749	0.6081	0.2661
$\sigma(Q^p)$	0.2706	0.1220	0.1967	0.3092	0.1830	0.1940

[a]The units $m^{1.5}s^{-1}$ come from $m^3s^{-1}(m^2)^{0.75}$, expressing $Q=\mathcal{Q}/A^{0.75}$ as noted in the text (section 2).

s and t are indices for space (catchment) and time (year), and the superscript p in $\mathcal{Q}$ refers to "peak." The number of catchments considered in the study is $n_s=804$ and the number of years $n_t=33$. Additional information regarding each catchment includes its area, geographical coordinates, mean elevation, and hydroclimatic region. We are interested in the scale-independent effect of precipitation on floods, so that the flood sensitivity will be invariant with regards to catchment size. Therefore, given the proportionality relation between flood peak magnitudes and catchment areas up to the power of 0.75 in Austria ($\mathcal{Q}^p_{s,t} \propto A^{0.75}$) [*Merz et al.*, 2009], $\mathcal{Q}^p_{s,t}$ is rescaled (divided) by that factor, yielding a matrix of specific flood peak magnitudes, $Q^p_{s,t}=\mathcal{Q}^p_{s,t}/A^{0.75}$. (Note the notation difference between Q and $\mathcal{Q}$.) Here and henceforth in this document, the expression "specific flood peaks" (or simply "flood peaks") shall refer to $Q^p_{s,t}$.

Basic statistical properties of $Q^p_{s,t}$ are presented in Table 1: the spatiotemporal mean $\mu(Q^p_{s,t})$ and standard deviation $\sigma(Q^p_{s,t})$, for Austria and each of its five hydroclimatic regions. Higher means are observed in the mountainous regions of Central and Northern Alps and lower for the Northern and Eastern Lowlands, consistent with the former being wetter regions and the latter drier ones. The Southern Alps, despite being mountainous, are predominantly drier than other Alpine areas, as it is often on the leeward side of the Alpine range in terms of dominant atmospheric circulation patterns.

The data on flood peaks are then processed in terms of sorted spatial and temporal means of precipitation. The practical procedure can be summarized as follows.

2.2.1. Setting the Space-Related Axis

The annual accumulated precipitation data $P_{s,t}$ are averaged over all years n_t for each catchment s, yielding an n_s-dimensional array of mean annual precipitations (MAP), n_s being the number of catchments. This array is then sorted in ascending order, yielding a sorted array P_s of mean annual precipitations. This is then taken as our space-related axis. In practice, this corresponds to sorting catchments from the driest to the wettest in terms of precipitation.

2.2.2. Setting the Time-Related Axis

Being n_t the number of years, an n_t-dimensional array is produced containing, for each year t, the spatial average of the yearly accumulated precipitations over all catchments, hereby called mean regional precipitation (MRP). This is then sorted in ascending order, yielding a sorted array P_t of MRP, our time-related axis. In practice, this corresponds to sorting years from the driest to the wettest in terms of precipitation.

2.2.3. Sorting Flood Peaks With Respect to the Axis in (1) and (2)

We sort $Q^p_{s,t}$ by increasing MAP and MRP, i.e., along the space-related (P_s) and time-related axes (P_t), in order to produce surface plots of the flood peaks with respect to increasingly wetter catchments and years. These are depicted in the results section of this paper (section 5).

2.3. Spatiotemporal Sensitivity

At this stage, we analyze the joint spatiotemporal sensitivity of the flood peaks with respect to precipitation (P). The joint sensitivity is given by the gradient:

$$\nabla_P(Q^p_{s,t})=\left(\frac{\partial Q^p_{s,t}}{\partial P_s},\frac{\partial Q^p_{s,t}}{\partial P_t}\right) \tag{1}$$

We are interested in geometric variations (ratios) of flood peaks with respect to this precipitation. Therefore, we begin by considering the $(P_s, P_t, Q^p_{s,t})$ space in logarithmic scale (of base-10), hereby denoted as

$(\tilde{P}_s, \tilde{P}_t, \tilde{Q}^p_{s,t})$. Then, we estimate the gradient with a first-order Taylor approximation surface to $\tilde{Q}^p_{s,t}$ with respect to $(\tilde{P}_s, \tilde{P}_t)$, by estimating the median gradients in space and time. The joint spatiotemporal sensitivity of flood peaks in logarithmic scale can then be drawn from:

$$\Delta_{\tilde{P}}(\tilde{Q}^p_{s,t}) = \alpha \Delta \tilde{P}_s + \beta \Delta \tilde{P}_t \tag{2}$$

Here α and β are median gradients denoting, respectively, the coefficients of spatial and temporal sensitivity of flood peaks to precipitation.

The natural-scale flood peaks and precipitation values can then be straightforwardly retrieved by exponentiating equation (2), yielding:

$$R_P(Q^p_{s,t}) = R^{\alpha}(P_s) \cdot R^{\beta}(P_t) \tag{3}$$

where $R(\cdot)$ denotes the ratio of variation: e.g., $R(Q^p_{s,t}) = \exp_{10}(\Delta \tilde{Q}^p_{s,t})$.

In order to enable a broader application to less monitored regions, this methodology has been devised bearing data sparse regions in mind. First, only annual flood peaks and annual rainfall totals are needed which are available at many stations around the world. Second, the median of all gradients was used for estimating α and β even if simple gradients would have sufficed in the particularly data-dense case of Austria.

Time sensitivity could potentially be affected by moisture storage between years (carryover), a process that would not be expressed in the space domain. In order to identify whether any carryover effects are at play reducing temporal gradients of flood peaks, the spatiotemporal sensitivities are recalculated over subsets with multiyear spacings of 1–5 years. This procedure yields similar results to those using the complete data sets, thus effectively ruling out carryover effects.

With the spatiotemporal sensitivity coefficients α and β at hand, symmetry properties of the flood response to precipitation can be evaluated along with signs of coevolution.

3. Symmetry and Coevolution

3.1. Challenges to Space-Time Symmetry

Space-time symmetry is often assumed in statistical analysis of spatially distributed geophysical time series [e.g., *Skøien and Blöschl*, 2006; *Harman et al*., 2011]. Symmetry assumptions are often grounded on the Taylor hypothesis [*Taylor*, 1938], which consists of a relation between the time variation of a flow at a fixed point in a streamline and the spatial codependence between the flow changes at two fixed points in the same stream. The application of the Taylor hypothesis, originally formulated with wind flow in mind, only legitimates space-for-time substitution to be conducted along the same stream, e.g., relating upstream to downstream gradients with temporal evolution at a given position along the stream. Extension to multiple streams will require relationships between their dynamical properties to be taken into account (e.g., rate of coevolution). Therefore, care must be exerted when applying this hypothesis to the geostatistical space-time analysis, as different streams can come into play with different dynamical properties.

Another common assumption supporting space-time symmetry lies on the assumed ergodicity of the physical system at play, whereby long-term temporal statistics are taken as corresponding to ensemble averages over the state space, leading to space-time symmetry. However, the required time scale for all possible states and interactions to be explored in macroscopic hydrological systems may be too large for the ergodic hypothesis to actually be valid, i.e., for statistics over space to be equivalent to (and thus tradable with) those over time. Moreover, the dissipative nature of such systems can effectively pose a natural barrier to symmetry, as the system may reach thermodynamic equilibrium without having had the time to venture across the whole phase space.

Symmetry breaks are ubiquitous in nature, such as in synoptic storm formation with self-organization of evenly distributed cloud patches into coherent, spiral storm structures with clear rotational direction, spontaneous magnetization or transition from paramagnetism to ferromagnetism in metal substances in equilibrium [*Prigogine and Nicolis*, 1967], and Lorentz symmetry breaking in string theory [*Kostelecký and Samuel*, 1989].

Asymmetries in the space-time sensitivities of floods to precipitation could arise from nonlinear interactions between processes acting at different spatiotemporal scales, leading to inhomogeneous controls being exerted across regions. The interplay between climate and landscape leads to different patterns of interference in different spatial and temporal scales, with different climate controls and different landscape resistances at play leading to further "speciation" of the environment. In fact, catchments can evolve at different paces and develop different features depending on the drivers acting over them (e.g., climate-related processes), and on the resistance their landscape poses to such drivers. Even considering a similar pair of processes, say precipitation and landscape formation, their interplay can be exerted at different time scales depending on climate and geological properties. For instance, a catchment with erodible soil will feature faster erosion under similar precipitation characteristics to those over a catchment with bedrock; likewise, considering two catchments with similar geology, the one with higher and stronger precipitation will undergo faster erosion than the one with milder precipitation patterns.

All in all, the relationship between the properties of different catchments across a region can evolve in time. This in turn means that the space-related coordinates (catchments) in the framework may exhibit time dependence, as landscapes can coevolve with climate-related mechanisms. That way, coefficient differences and thus asymmetries in the space-time sensitivities could arise in a scenario of landscape-climate coevolution.

3.2. Coevolution and Space-Time (A)Symmetry

In the present subsection, we establish a quantitative relationship between coevolution and space-time symmetry, leading to the correspondence between coevolution and space-time *asymmetry* or, equivalently, between space-time symmetry and the lack of coevolution. The key to the problem is the understanding that the coordinates representing space and time are not necessarily independent from each other. In the present study, the space is represented by catchments and their physical properties; not by clean axis on an abstract Euclidean space. If the distance between coordinate points change with time (e.g., if the difference between catchments in terms of their properties changes), then in the analysis of the dynamics, a term of dependence of space on time will thus be included.

The time evolution of the quantities $P_{s,t}$ and $Q^p_{s,t}$ is thus written as total time derivatives in the following form:

$$\frac{dP_{s,t}}{dt} = \frac{\partial P_{s,t}}{\partial t} + \frac{\partial P_{s,t}}{\partial s}\frac{ds}{dt} \tag{4}$$

$$\frac{dQ^p_{s,t}}{dt} = \frac{\partial Q^p_{s,t}}{\partial t} + \frac{\partial Q^p_{s,t}}{\partial s}\frac{ds}{dt} \tag{5}$$

Note that the cardinality of $Q^p_{s,t}$ and $P_{s,t}$ is the same as that of the underlying space-time (s, t), therefore they are dense in that spatiotemporal platform.

Space-time symmetry occurs when $ds/dt = 1$. In a coevolving scenario, this term can vary, as the spatial coordinates, here given by catchment properties, will no longer be invariant.

Let the operators $E_s[\cdot]$ and $E_t[\cdot]$ denote, respectively, spatial and temporal means. Applying these operators to $P_{s,t}$ and $Q^p_{s,t}$ and taking into account equations (4) and (5), the relation between means over space and over time becomes:

$$E_t[P_t] = \frac{ds}{dt}E_s[P_s] \tag{6}$$

$$E_t[Q^p_t] = \frac{ds}{dt}E_s[Q^p_s] \tag{7}$$

where $P_t = E_s[P_{s,t}]$, $P_s = E_t[P_{s,t}]$, $Q^p_t = E_s[Q^p_{s,t}]$, and $Q^p_s = E_t[Q^p_{s,t}]$.

The equations (6) and (7) show that, though related, spatial and temporal statistics are not necessarily the same. They are related to one another by the celerity ds/dt. Therefore, space-for-time trading requires taking

this term into account. Considering the ratio between states at time t with those at time t_0, the dependence of Q^p on P_s and P_t derives from equation (3) as:

$$Q_t^p = P_t^\beta \frac{Q_{t0}^p}{P_{t0}^\beta} \tag{8}$$

$$Q_s^p = P_s^\alpha \frac{Q_{s0}^p}{P_{s0}^\alpha} \tag{9}$$

The space-time dependence can then be derived from equations (6)–(9) as:

$$\frac{ds}{dt} = E_s \left[\frac{P_s}{P_{s0}}\right]^{\alpha-\beta} \tag{10}$$

In particular, for $\alpha=\beta$, we have $ds/dt=1$, corresponding to space-time symmetry and no coevolution, as noted before. A practical coevolution index $\mathcal{E}$ can be defined from equation (10) as:

$$\mathcal{E} = \widetilde{\left(\frac{ds}{dt}\right)} E_s^{-1} \left[\tilde{P}_s - \tilde{P}_{s0}\right] = \alpha - \beta \tag{11}$$

where $\tilde{\cdot}$ denotes $\log_{10}(\cdot)$ as in the previous section. This relation quantifies coevolution in terms of the asymmetry between the spatial and temporal sensitivities (α and β). In particular, the space-time symmetry and absence of coevolution is then expressed as $\mathcal{E}=0$.

Note that, while coevolution is associated to space-time asymmetry, it does not invalidate space-for-time substitution. On the contrary, it enables it by establishing an effective link between space and time (the aforementioned celerity ds/dt), without which such operation would not be legitimate.

3.3. Gauging Coevolution From Landscape-Climate Spatial Codependence

The process of landscape-climate coevolution has a time scale orders of magnitude larger than the time window used for the data of the present study. Still, the current state of the catchments and statistics on precipitation and floods can be used to infer whether coevolution has taken place, by analyzing the degree of spatial statistical codependence between climate and catchment properties. In fact, coevolution is evaluated not from data in the time domain at decadal scales but rather from the spatial domain, looking at the legacy of what a millennial-scale coevolution has had on the spatial (catchment) statistics.

While statistical codependence is not causation, it may provide hints on possible links between processes leading to the observed distributions of landscape and climate properties. For instance, strong correlations suggest the existence of some interconnection between landscape and climate, whereas the absence of such relations suggest that landscape and climate processes may not be dependent on each other. We note, however, that null correlations do not necessarily imply independence.

At this stage, we look at signs of landscape-climate codependence that may suggest whether landscape-climate coevolution has been taking place. We do so by evaluating statistical codependence measures between hydroclimatic and orographic properties, namely between the mean annual precipitation (P_s) and arithmetic mean catchment elevation (H), using two approaches: on one hand, Spearman Correlations [*Wilks*, 1995], measuring the degree of monotonic association between variables; on the other, Information Correlations [*Pires and Perdigão*, 2007], a measure of nonlinear codependence based on the information-theoretical measure of Mutual Information and estimated using Maximum Entropy Anamorphoses [*Pires and Perdigão*, 2013]. The results are presented in section 5.3 and further methodological details on Information Correlation are provided in Appendix A.

Having addressed descriptive indicators of landscape-climate coevolution, the dynamics supporting such indicators are addressed in the next section.

4. Understanding Coevolution: A Dynamical Approach

4.1. Processes and Feedbacks at Play

By having investigated signs of coevolution in the light of information retrieved from the data sets in the previous section, it is now important to understand those signs under dynamical grounds, by relating statistical signatures with underlying physical mechanisms as represented by a dynamical model. In the present section, a simple model is built that dynamically relates the changing climatology of precipitation with that of the mean catchment elevation through a feedback mechanism, in an attempt to represent and understand catchment coevolution with climate dynamics. In this section, "precipitation" shall thus refer to its climatology, *not* to a weather event. Therefore, the coevolution link with landscape will be established between asymptotic rather than transient features of climate. The model is formally simple in order to focus on a key feedback mechanism between climate and landscape, while retaining enough basic realism to allow for the model-based results to fairly represent data-retrieved information.

The model structure is based on physical arguments consistent with observed landscape formation and climate-related controls [e.g., *Marsh and Kaufman*, 2013; *Gregory and Walling*, 1973]. Three key arguments are hereby considered: (a) slow-fast landscape-climate feedbacks; (b) limited resources (carrying capacity); and (c) stable states: dry lowlands and wet highlands.

4.1.1. Slow-Fast Landscape-Climate Feedbacks

In general, provided there is enough precipitable water in the atmosphere, a slow increase in elevation is associated with a fast increase in precipitation. An increase in precipitation leads to increased runoff and erosion, which in turn contributes to a decrease in elevation. This thus corresponds to a decrease in mountain mass, which then leads to passive uplift (from buoyancy of the solid crust floating on the mantle geofluid). Tectonic uplift is not being considered here, as the observed uplift in the study area is primarily passive, climate driven, rather than a consequence of active orogenic mechanisms [*Champagnac et al*., 2009]. Mountain elevations increase due to uplift, so does precipitation, triggering the process loop all over again.

4.1.2. Limited Resources (Carrying Capacity)

The aforementioned feedback loop will last only up to a certain extent, depending on resource availability (e.g., precipitable water in the atmosphere) and geological constraints effectively controlling uplift. At this point, let us focus on the water availability and take the reasonable assumption that the uplift mechanism will stay fundamentally invariant (in such a way that its response to mountain mass loss stays coherent). We can then define a carrying capacity effectively limiting the amount of precipitation, effectively grinding the positive feedback between landscape and precipitation to a halt, expressed as a saturation level in precipitation.

4.1.3. Steady States: Dry Lowlands and Wet Highlands

At high elevations, the system can be locked on a state whereby precipitation is high albeit not increasing further, at a high (though not increasing) elevation. As precipitation ceases to increase, so does weathering, therefore elevation is not put under additional erosive stress. At low elevations an increase in precipitation and consequently in weathering and erosion will not lead to substantial uplift, as there is no major elevation and mass loss. Rather, as elevation decreases, precipitation tends to decrease as well, while still eroding the landscape (albeit gradually less). At some stage, the landscape tends to become flatter and drier, converging to a flat, dry setting where it stays locked in a negative, stabilizing feedback. These upper and lower stabilizing limits in precipitation as it interacts with the landscape suggest the existence of two steady states in the landscape-climate system: on one hand, a {highland, wet} state, and a {lowland, dry} one.

4.2. A Simple Dynamical Model of Coevolution

The landscape-climate coevolution model is set as a slow-fast dynamical system, which implies two distinct time scales. On one hand, there is a slow time scale, millennial, at which landform evolution processes take place. The

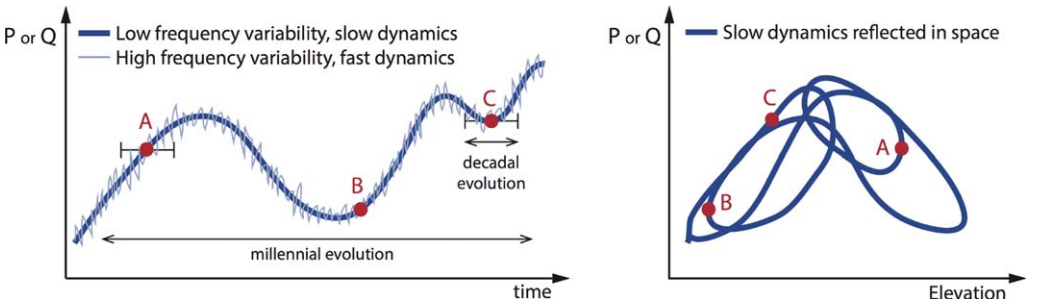

Figure 1. Schematic of slow-fast dynamics and landscape-climate coevolution. The left plot schematically depicts the short and long-term evolution of precipitation (P) or flood peaks (Q). The slow dynamics take place at the millennial scale and can be seen as a moving average of the fast dynamics over time windows at the decadal scale (33 years in the present study). The right plot depicts the slow, millennial-scale dynamics of P or Q with Elevation, i.e., its phase space trajectory. It thus depicts a spatial codependence corresponding to the long-term landscape-climate coevolution. The red dots represent the short-term average of the fast dynamics of P or Q for different stages in the millennial evolution corresponding to the state of landscape-climate coevolution at catchments A, B, and C.

evolution of catchment elevation (surrogate for landscape evolution) and that of the precipitation climatology (surrogate for climate change) are set in this context. This is thus the time scale at which coevolution takes place. On the other hand, there is a fast time scale at which precipitation adjusts to slow, gradual changes in elevation. The dynamics taking place in the sampled temporal domain of 33 years are set in this context. Figure 1 depicts this rationale.

The dynamical processes and feedbacks outlined in section 4.1 suggest a dynamical model of coevolution in logistic form. In fact, logistic dynamical systems take into account dynamical couplings representing feedbacks between slow and fast physical processes (section 4.1.1), moderated by a carrying capacity (section 4.1.2) dependent on the slow variable (here, on elevation) and limiting the growth of the fast variable (here, precipitation). The time scales associated to the fast and slow processes at play here are, respectively, decadal and millennial (dozens to hundreds of thousands of years). Logistic systems also provide grounds for understanding the negative feedbacks that take place around stable states of the dynamical process (section 4.1.3).

We are now in position to propose a simple dynamical model of landscape-climate coevolution, taking as the key climate variable the precipitation climatology (P) or mean annual precipitation, and as the landscape variable the mean catchment elevation (H). The transient precipitation climatology for each catchment will tend toward a limiting state (P_C) as climate adjusts to incremental changes in H. The model-generated phase space portrait (P_C, H) will be compared with the data-based joint distribution of mean annual precipitation and mean catchment elevation in section 5.4.

Since we are interested in how climate changes in articulation with the landscape and vice versa (coevolution), we consider P as a function of H, aside from all other controls $\mathcal{O}$:

$$\frac{dP}{dt} = f(P, H, \mathcal{O}) \tag{12}$$

where f is a generic nonlinear function.

In order to focus our attention on climate-landscape feedbacks, we neglect at this stage the explicit influence of other controls as compared to that of elevation, by introducing the constraint: $|\frac{\partial P}{\partial \mathcal{O}}| \ll |\frac{\partial P}{\partial H}|$. The dynamical system in equation (12) will thus be approximated by $\frac{dP}{dt} = f(P, H)$. We now explicit f by introducing the following nonlinear dynamical model of landscape-climate coevolution in logistic form:

$$\frac{dP}{dt} = \gamma P\left(1 - \frac{P}{P_C}\right) \tag{13}$$

where:

$$P_C = \begin{cases} 1 - \exp\left(-\mathcal{E}\dfrac{H}{H_l - H}\right), & \text{if } H < H_l \\ \exp\left[\mathcal{E}\left(\dfrac{H_l - H}{H_l}\right)\right], & \text{if } H \geq H_l \end{cases} \tag{14}$$

The term P_C, through which H interacts, i.e., coevolves with P is the limit to which P tends on its transient evolution, as noted above. It represents the carrying capacity of the system, expressing the limitation on the amount of precipitation physically possible given constraints on available resources (e.g., humidity, precipitable water). This is the term where coevolution $\mathcal{E}$ (equation (11)) is explicitly taken into account. As for γ, with dimensions $[t^{-1}]$, it denotes the rate of transient evolution of P toward its limiting state P_C. As such, it also accounts for how fast P responds to perturbations (i.e., to changing conditions), as it is related to the largest Lyapunov exponent of the system (i.e., the highest rate of divergence in trajectories originated in arbitrarily close, albeit not equal, initial conditions). It is a climate-specific coefficient, associated to fast-responding atmospheric dynamics and internal climate variability. The adimensional term $\mathcal{E}$ regulates the rate of coevolution between P and H, expressing the sensitivity of the former to the latter. It corresponds to the term defined in equation (11). The terms γ and $\mathcal{E}$ thus regulate two different time scales: γ for that of the fast, decadal scale of the dynamics of P on its transient evolution toward P_C; $\mathcal{E}$ for the slow, millennial time scale at which the landscape-climate coevolution takes place as represented by the codependence between P_C and H in equation (14). The incremental changes in H are much slower than the atmospheric response; therefore, P can always reach P_C in all stages of coevolution. The changes in P_C will thus allow us to track down the coevolution process.

By analyzing the steady states of equation (13) (by equating it to zero), two such states can be identified, as noted in the previous subsection: on one hand, a {lowland, dry} state, whereby a dry climate occurs on lowlands; on the other hand, a {highland, wet} state, whereby a wet climate occurs on elevated areas. The former is represented by $P_C = 0$, occurring when H tends to 0, corresponding to the system being locked on a dry climate state on lowlands. The latter is represented by $P_C = 1$ (maximum capacity), occurring if the elevation would reach a level $H = H_l$. Up to that level, as moist air would be advected uphill, it would cool down and condense, leading to higher cloud formation and ultimately precipitation. While water would be available in the air parcel, higher altitudes would correspond to higher precipitation. This would continue until the water content in the rising air parcel would no longer be enough to sustain that trend, rather being progressively depleted. Therefore, above that level H_l available precipitable water would decay with increased elevation [*Salby*, 1996; *Salby*, 2012], leading P_C to do so as well.

The solution of equation (13) is obtained by integration as:

$$P(t) = \frac{P_C P_0 \exp(\gamma t)}{P_C + P_0 \exp(\gamma t - 1)} \tag{15}$$

where $P_0 \equiv P(t = 0)$. γ and P_C are taken time invariant in the integration process, as they do not significantly vary in the decadal time scale at which P responds for each incremental change in H.

A feedback mechanism between two variables is inherently bidirectional, albeit not necessarily symmetric. By having established the way H influences P, the way it is *influenced* can now be defined as follows:

$$\frac{dH}{dt} = \sigma_P \tag{16}$$

where σ_P represents the sensitivity of H on P via erosive and passive uplifting processes as explained in section 4.1.1.

Equation (16) expresses H as a surrogate for the slow time scale, therefore the codependence between P_C and H in equation (14), albeit diagnosable in space, actually represents a long-term, slow dynamical process at the millennial scale. Coupled with the fast dynamics (equation (13)) prescribing the transient evolution of

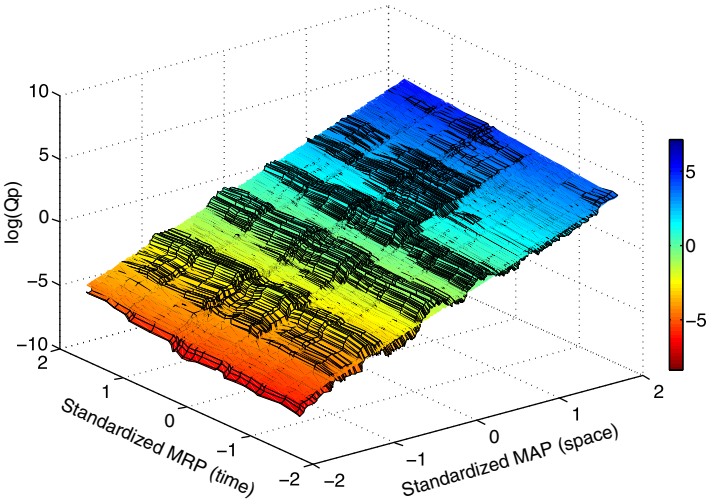

Figure 2. Spatiotemporal sensitivity of flood peaks to precipitation for Austria as a whole, depicted as surface plots of the flood peaks $\tilde{Q}^p_{s,t}$ with respect to precipitation sorted along space, mean annual precipitation (MAP), and time, mean regional precipitation (MRP). Also shown the best gradient fitting plane, the slopes of which are given by the median of all gradients along space and time. The axis are standardized and given in base-10 logarithmic scale.

P toward P_C adjusting to the slow variable H, it gives us a minimalistic slow-fast dynamical system representing landscape-climate evolution.

Having established a dynamical model for P, a corresponding model for mean annual flood peaks Q^P can now be derived. For that purpose, we denote $\kappa = \partial Q^P / \partial P$, take $Q^P = P^\kappa Q^p_{t0} / P^\kappa_{t0}$ analogously to equation (8) and combine with (13) to obtain:

$$\frac{dQ^p}{dt} = \gamma \kappa Q^p \left[1 - B(Q^p)^{1/\kappa}\right] \quad (17)$$

with

$$B = \frac{P_0}{P_C (Q^p_0)^{1/\kappa}} \quad (18)$$

By inspecting equation (17), some interesting cases arise. For instance, when $\kappa = 1$ it becomes a logistic equation akin to equation (13). When $\kappa = 2$, equation (17) becomes a bistable system [*Nicolis et al.*, 2009], which enables regime shifts without changes in external controls (i.e., they can arise from the natural dynamics of the system). Therefore, if the present model exhibits a bistable configuration, an autonomous regime shift can occur between, say, a {*low*, *dry*} and a {*high*, *wet*} regime. This differs from a logistic configuration, whereby once the system settles on a steady state, it tends to be locked there due to negative feedbacks.

Note that κ refers to the sensitivity of mean annual flood peaks to mean annual precipitation, where the means are aggregates over a multidecadal period. This term should not be confused with the year-to-year time sensitivity of annual flood peaks to annual precipitation, given by β. Rather, κ is related to α as both refer to sensitivities of mean annual flood peaks to mean annual precipitation. In fact, α is actually the median of all gradients κ.

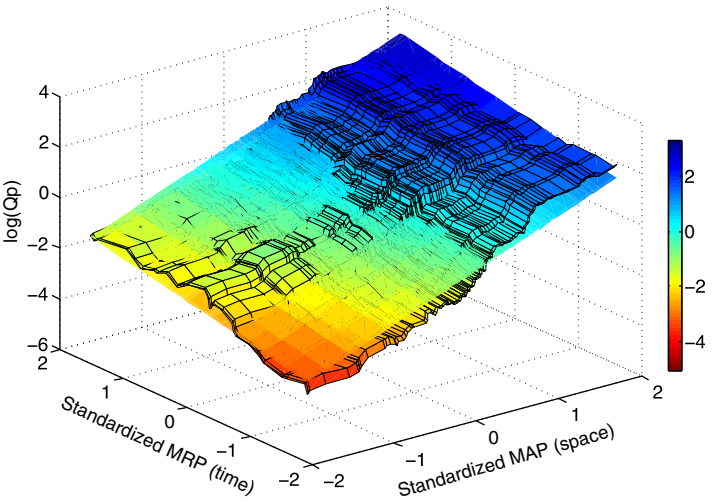

Figure 3. As Figure 2, now for region 3 of Austria (Northern Alps).

5. Results and Discussion

5.1. Spatiotemporal Sensitivity Results

The spatiotemporal sensitivity of flood peaks to precipitation has been assessed for the aforementioned five Austrian regions, along with Austria as a whole. The surface plots of the flood peaks $\tilde{Q}^p_{s,t}$ with respect to precipitation sorted along space ($\tilde{P}_s$), mean annual precipitation, and time ($\tilde{P}_t$), mean regional precipitation, are depicted in Figures 2–4, corresponding,

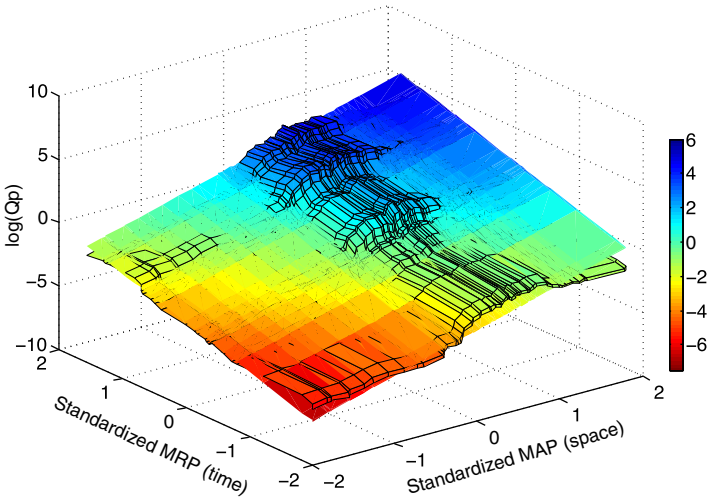

Figure 4. As Figure 2, now for region 5 of Austria (Eastern Lowlands).

respectively, to all Austrian catchments, region 3 (Northern Alps), and region 5 (Eastern Lowlands). These plots are complemented with the best gradient fitting plane, the slopes of which are given by the median of all gradients along space and time, as noted above. The axis are standardized and given in base-10 logarithmic scale; therefore, the surface plots are also in a logarithmic scale, where the linear slope actually corresponds to an exponential relation between $Q^p_{s,t}$ and $P_{s,t}$. Spatial and temporal sensitivities can also be seen on the color gradients in the aforementioned figures. There, the color scale represents values of $Q^p_{s,t}$, ranging from red for lowest values to blue for the highest. Higher sensitivities across space or time correspond to sharper color changes across those directions.

Table 2 presents the spatiotemporal sensitivity coefficients corresponding to the slopes from the planes depicted in Figures 2–4, along with those of the regions whose sensitivities had not been depicted. The coefficients α and β refer to the sensitivity in space and time, respectively. The sensitivity values are provided with the 95% confidence bounds, expressing the degree of uncertainty in the estimation of spatial and temporal slopes.

The spatiotemporal depiction of the sensitivity of floods to precipitation allows us to compare the relative contributions and symmetry properties of the spatial and temporal sensitivities. The results show an overall greater sensitivity of flood peaks to precipitation over space than over time in Austria. In fact, α is greater than β in the country as a whole (indicated as "All"). These sensitivity indicators and their difference can be better understood if we note that, for instance, a space sensitivity coefficient of 2.31 means that a 10% increase (decrease) in precipitation over space (catchments) leads to an increase (decrease) of about 23% in flood peaks. Analogously for time, a time coefficient sensitivity of 0.61 means that a variation of 10% in precipitation over time leads to a same-signal variation of only about 6% in flood peak magnitudes.

The greater sensitivity with regards to space may be due to the coevolution of the catchments, in a feedback between precipitation and catchment properties, whereby: (1) catchments undergoing higher precipitation will tend to become shallower due to erosion and consequent loss of soil depth and ultimately elevation; (2) those catchments with lower precipitation will have less erosion and be prone to developing deeper, flatter soils with higher storage capacity and lower risk of posing an obstacle to atmospheric flow, which in turn reduces the risk of precipitation, namely of orographic origins. Areas dominated by synoptic-scale precipitation will, however, not exhibit significant coevolution, as synoptic systems to not respond to catchment characteristics, thus breaking the feedback loop.

Table 2. Spatiotemporal Sensitivity Coefficients α and β for Austria and Its Five Hydroclimatic Regions

		Hydroclimatic Region					
			Region 1	Region 2	Region 3	Region 4	Region 5
Domain	Coefficient	All Austria	C. Alps	S. Alps	N. Alps	N. Lowlands	E. Lowlands
Space	α	2.31 ± 0.27	0.78 ± 0.10	1.41 ± 0.05	1.26 ± 0.13	2.11 ± 0.06	1.84 ± 0.14
Time	β	0.61 ± 0.11	0.75 ± 0.14	0.52 ± 0.06	0.52 ± 0.08	1.04 ± 0.11	1.57 ± 0.21

Table 3. Rates of Coevolution $\mathcal{E}$ for Austria and Its Five Hydroclimatic Regions

	Hydroclimatic Region					
		Region 1	Region 2	Region 3	Region 4	Region 5
Rate of Coevolution	All Austria	C. Alps	S. Alps	N. Alps	N. Lowlands	E. Lowlands
$\mathcal{E}$	1.70 ± 0.38	0.03 ± 0.24	0.89 ± 0.11	0.74 ± 0.21	1.07 ± 0.17	0.27 ± 0.35
Interpretation	Multiple states	Stable {high,wet}	Coevolving	Coevolving	Coevolving	Stable {low,dry}

By looking at each hydroclimatic region individually, the results can be divided into two main categories. On one hand, there is greater sensitivity of flood peaks to precipitation over space than over time in regions 2, 3, and 4, corresponding, respectively, to Southern Alps, Northern Alps, and Northern Lowlands. On the other hand, in regions 1 and 5 (Central Alps and Eastern Lowlands, respectively), the equality between spatial and temporal sensitivities is within the error margins. This means that there is space-time symmetry in the flood peak sensitivity to precipitation in the Central Alps and Eastern Lowlands.

The difference between spatial and temporal sensitivities in individual regions is not as large as for Austria as a whole, as the overall country encompasses the biggest range of variability in hydroclimatic properties and sensitivities. In fact, in Austria the inter-regional variability (i.e., among different regions) is higher than the intra-regional variability (comparing catchments within each region).

5.2. Symmetry and Coevolution Results

The space-time symmetry in relatively stable hydroclimatic regions (1 and 5) is consistent with previous studies mostly focusing on nontransient areas (e.g., *Harman et al*. [2011], who have taken mainly catchments east of the Rocky Mountains). The Austrian regions where symmetry does not hold are essentially areas where transient hydrogeological processes are at play, such as changes in erosion and its weathering effects. As long as there are catchments undergoing transient processes, equilibrium is yet to be reached, therefore the ergodic hypothesis is not yet legitimate in such cases. The key to symmetry breaks is the ongoing landscape-climate coevolution, visible in transient areas such as regions 2, 3, and 4 of Austria. These evolving regions exhibit streams whose properties may be evolving at different rates, both due to different atmospheric currents and to the heterogeneity of climatic controls and landscape responses. Symmetry is expected once equilibrium has been achieved, but that is seemingly not yet the case in those regions.

The space-time symmetry of regions 1 and 5 and asymmetry in regions 2, 3, and 4 is thought to be associated to the degree of hydrogeological stability of the corresponding regions. In fact, while the former (regions 1 and 5) are stable, region 1 being on high lands with shallow soils and high precipitation and region 5 on lowlands with thick soils and low precipitation, the latter (regions 2 to 4) are undergoing landscape-climate coevolution, with changing catchment properties (e.g., changing soil thickness and thus storage capacity due to erosion) and coevolving climate-related properties (precipitation patterns change with landscape changes in such properties as elevation and slope). The rates of coevolution between landscape and climate are not invariant, as different soil and overall geological properties pose different levels of resistance to climate forcings. These, in turn, are not homogeneous over the country, as precipitation is affected not only by large-scale synoptic patterns, but also to more regional-scale orographic effects. The heterogeneity in climate-related forcings and landscape-related resistance and the coevolution between these processes may thus explain different characteristic celerities of catchment coevolution, effectively breaking the Taylor's hypothesis. On the thermodynamic perspective, regions 2 to 4 may be transients in terms of geological time scales of landscape evolution, not having yet reached an equilibrium state, therefore the ergodic hypothesis of space-time symmetry and interchangeability in statistical analysis may not hold.

These statements are further supported by the coevolution indicators $\mathcal{E}$, presented for Austria and its five hydroclimatic regions in Table 3.

5.3. Landscape-Climate Spatial Codependence Results

In order to gauge landscape-climate codependence, let us look at the spatial correlations between catchment properties (e.g., elevation) and hydroclimatic variables (mean annual precipitation and flood peaks), presented as Spearman Correlations in Table 4 and Information Correlations in Table 5.

Table 4. Statistical Codependence Among Orographic Properties and Hydroclimatic Variables[a]

	Hydroclimatic Region					
Spearman Correlation	All Austria	Region 1	Region 2	Region 3	Region 4	Region 5
$\rho(P_s, \tilde{Q}_s^p)$	0.880*	0.586*	0.795*	0.843*	0.863*	0.756*
$\rho(P_s, H)$	0.275	0.082	0.195	0.135	0.262*	0.042
$\rho(\tilde{Q}_s^p, H)$	0.252	0.063	0.177	0.140	0.239*	0.036

[a]H stands for mean catchment elevation. Statistically significant correlations at 95% confidence level are marked with an asterisk (*).

Table 4 brings out two distinct behaviors in the codependence between hydroclimatic and orographic properties. On one hand, weak codependence for regions 1 and 5, suggesting that hydroclimatic and orographic processes are not significantly related, i.e., it is unlikely that coevolution takes place. This is consistent with region 1 being in a stable {high, wet} state and region 5 in a stable {low, dry} state, as discussed above.

On the other hand, regions 2, 3, and 4 exhibit stronger codependence between hydroclimatic and orographic properties, which suggests some degree of dependence in associated processes and thus a possibility that coevolution takes place in those regions. These results are consistent with the coevolution diagnosis established from the asymmetry between spatial and temporal flood responses to precipitation as discussed above. They are also consistent with knowledge that in those regions there is ongoing soil dynamics influence by climate-related factors such as precipitation-driven erosion [e.g., *Gregory and Walling*, 1973].

The flood response in geologically stable areas may thus be mainly driven by atmospheric factors. These results are consistent with region 5 featuring essentially stable lowlands with dominant synoptic meteorological patterns and with region 1 having relatively bare soils with high erosive resistance, thus not favoring a scenario of landscape-climate coevolution. These also come in agreement with the similarities in the spatial and temporal sensitivities of floods to precipitation.

There is some codependence between hydroclimatic and landscape properties (about 15 to 20% correlation) in regions 2 and 3, where precipitation and flood peaks are highly correlated (above 98%). This suggests the existence of coevolution between precipitation and catchment attributes, as noted when analyzing the spatial sensitivity (α) and its difference with respect to the temporal one (β).

Unlike regions 2 and 3, in regions 1 and 5, the correlations between precipitation and floods are not that strong. The overlap between those correlations is thus minimal in regions 1 and 5, while significantly larger in regions 2 and 3. This overlap may be a better indicator of coevolution. In fact, an overlap suggests that the overlapping drivers are working together, rather than in disjunction.

As far as statistical significance is concerned, only the correlations between elevation and slope and those between precipitation and flood peaks are significant in all situations. The other correlations are only statistically significant in region 4 (Northern Lowlands).

The interpretations derived from the Spearman Correlations in Table 4 are further stressed by the Information Correlations on Table 5. In fact, these are higher and statistically more significant, while maintaining the overall relative differences when comparing regions with one another. The higher levels of codependence measured by the Information Correlation are explained by the more general nature of this measure, capturing not only monotonic relationships and retrieving the same information as a traditional correlation, but also retrieving

Table 5. Information Codependence Among Orographic Properties and Hydroclimatic Variables[a]

	Hydroclimatic Region					
Information Correlation	All Austria	Region 1	Region 2	Region 3	Region 4	Region 5
$\rho_I(P_s, \tilde{Q}_s^p)$	0.898*	0.741*	0.827*	0.854*	0.882*	0.799*
$\rho_I(P_s, H)$	0.729*	0.176	0.542*	0.483*	0.701*	0.198*
$\rho_I(Q_s^p, H)$	0.704*	0.189	0.538*	0.485*	0.692*	0.197*
Interpretation	Possible coevolution	Stable {high,wet}	Coevolving	Coevolving	Coevolving	Stable {low,dry}

[a]H stands for mean catchment elevation. The net Information Correlation already accounts for the correction of the residual mutual information. Statistically significant correlations at 95% confidence level are marked with an asterisk (*).

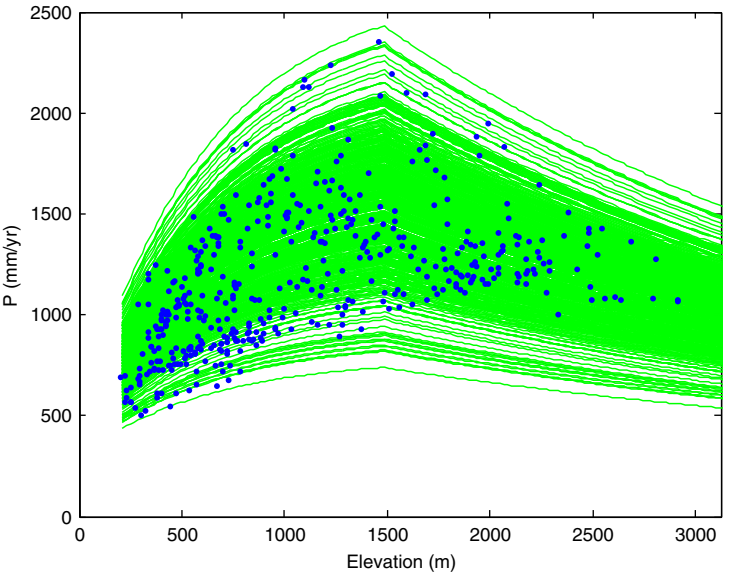

Figure 5. Depiction of the mean annual precipitation (P) (in mm/yr) with regards to mean catchment elevation. Blue dots represent P for each catchment, as retrieved from the observational data sets. The green lines represent the climatological phase space portrait of the dynamical model (equation (13)) (Precipitation versus Elevation), considering an ensemble of 500 realizations with varying initial conditions in P. The coevolution rate is $\mathcal{E}=1.70\pm0.38$.

information from nontrivial nonlinearities in the joint distribution of the variables under analysis. These advantages of the Information Correlation measure with regards to more traditional correlation measures are consistent with the results from *Pires and Perdigão* [2007] in the context of the dependence between large-scale atmospheric patterns and precipitation regimes in Europe.

Aside from the landscape-climate codependence, Tables 4 and 5 provide statistical relations between precipitation and flood peaks. As expected, they are very significant, with an overall Austria-wide Spearman Correlation of 0.880 and Information Correlation of 0.898. These results come in agreement with several studies that had shown strong correlations between flood and precipitation measures [e.g., *Farquharson et al.*, 1992; *Madsen et al.*, 1997; *Reed*, 1999; *Parajka et al.*, 2010].

5.4. Results From the Dynamical Model of Coevolution

In order to better understand the dynamics underneath coevolution, the data-based results are now compared with the information conveyed by the dynamical model introduced in section 4. For that purpose, the mean annual precipitation (P) and the mean annual flood peaks (Q^P) are depicted with regards to the mean catchment elevation (H) in Figures 5 and 6, respectively. In Figure 5, blue dots represent P for each catchment, as retrieved from the observational data sets, and the solid lines represent the phase space portrait of the dynamical model (equation (13)), considering an ensemble of 500 realizations with varying initial conditions in P. In Figure 6, blue dots represent Q^P for each catchment, also from the observational data sets, and the solid lines represent the phase space portrait of the dynamical model (equation (17)), considering an

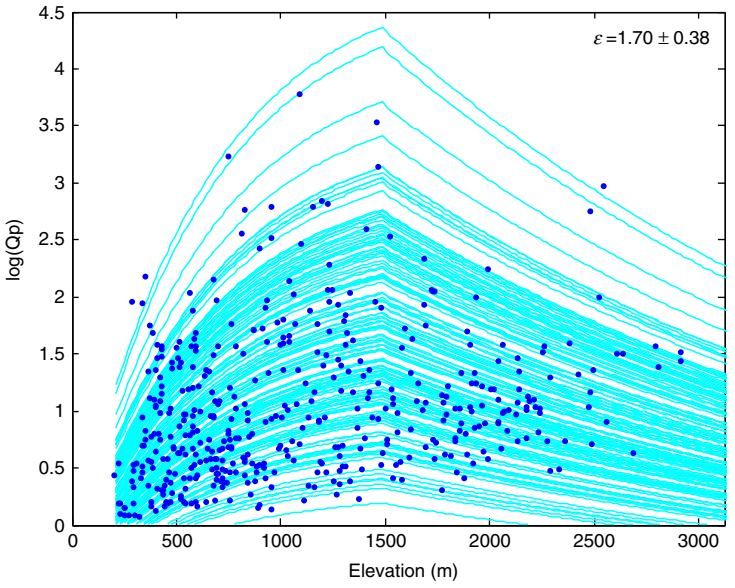

Figure 6. Depiction of the mean annual flood peaks (Q^P) (in log scale) with regards to mean catchment elevation. Blue dots represent Q^P for each catchment as retrieved from the observational data sets. The cyan lines represent the phase space portrait of the dynamical model (equation (17)), considering an ensemble of 150 realizations with varying initial conditions in Q^P. The coevolution rate is $\mathcal{E}=1.70\pm0.38$.

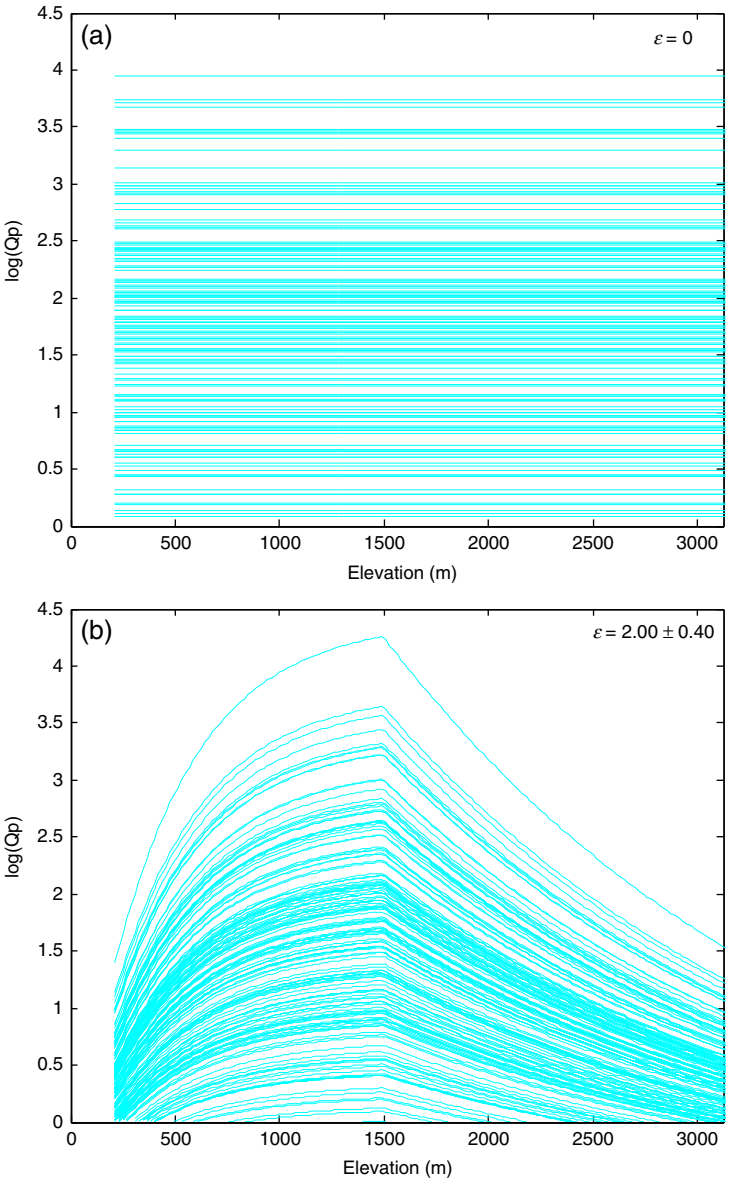

Figure 7. Depiction of the mean annual flood peaks (Q^P) (in log scale) with regards to mean catchment elevation, considering two model scenarios: (a) without coevolution ($\mathcal{E}=0$), and (b) with a coevolution rate of $\mathcal{E}=2.00\pm0.40$. The cyan lines represent the phase space portrait of the dynamical model (equation (13)), considering an ensemble of 150 realizations with varying initial conditions in Q^P.

ensemble of 150 realizations with varying initial conditions in Q^P and the range of values of $\mathcal{E}$ for all Austria as in Table 2.

By comparing the observational output (the dots) with the model output (lines) in Figure 5 it can be seen that the dynamical model (13) fairly represents the data distribution of the pair (Precipitation, Elevation). In fact, the P increase with H is captured by the model until a level $H_l=$ 1500 m. Above this level, the model depicts a decreasing P with increasing H and so does the data. Still, the scarcity of points at that stage only allows for an intuitively suggestive rather than a definitive diagnosis of data-model conformity.

The results are less clear for Q^P in Figure 6. In fact, the data distribution is so disperse that no clear pattern can be effectively attributable. Still, the model (17) cannot be ruled out as a possibility to represent and give meaning to the pair (Q^P, H). The rationale follows that of P, whereby an increase in this climatic variable promotes the occurrence of higher flood peaks and of Q^P overall, which in turn means that Q^P would follow the behavior of P to some extent. Still, because a given precipitation gives rise to a range of possibilities for flood peaks (including no floods at all), the spread in Q^P is naturally higher for a given H, as seen in Figure 6.

The slope of P with respect to H denotes the rate at which the former depends on the latter, expressed by $\mathcal{E}$ in the model. As explained in section 4.2, this corresponds to a rate of coevolution. Therefore, coevolution can be gauged from the slope of the graphs in Figures 5 and 6. The overall rate of coevolution for Austria is around 1.70, consistent with the correlations between H and P (section 3.3) and with the coevolution indicator gauged from the asymmetry between spatial and temporal sensitivities of floods to precipitation.

Two distinct hypothetical cases yielded by the dynamical model are now considered in Figure 7, taking ensembles of 150 initial conditions Q_0^P: on one hand, a scenario of no coevolution (Figure 7a); on the other,

the output of a coevolution with $\mathcal{E}=2.00\pm0.40$, slightly higher than the one considered in Figure 6. Figure 7a tells us that had coevolution been absent, P (and Q^P) would not depend on H, thus yielding a null evolution rate for all ensemble members. In fact, for each run, Q^P remains unchanged as H varies. These results are consistent with the evaluation of coevolution by landscape-climate codependence (section 5.3), which in this case is also null given the uncorrelated signatures depicted in this figure. As for Figure 7b, the model output resembles that in Figure 6, with an important exception: the rate at which Q^P varies with H is higher in Figure 7b, a result consistent with a higher coevolution rate in this case.

6. Conclusions

The results have shown that the spatial sensitivity of floods to precipitation exceeds that over time, in such a way that, given a 10% spatial increase in precipitation, there is a corresponding 23% increase in flood peaks, whereas given a similar 10% increase in precipitation over time, the flood peaks increase only about 6%.

The observed difference between sensitivities to space and time could not be attributed to year-to-year carryover, resulting in memory accumulation that would decrease gradients over time. This being said, we looked at whether the coevolution between climate and landscape could play a part. For that purpose, we began by looking at statistical relationships between climate and orographic properties as measured by Spearman and Information Correlations. While the former revealed modest yet significant relations for Austria (as it only accounts for monotonic relationships), the latter, based on the information-theoretical concept of Mutual Information, retrieved more significant information shared by climate and landscape-related properties, resulting in higher correlations. These relations are an indicator suggesting coevolution in the sense that they are a necessary, albeit not sufficient, condition for a coevolution diagnosis to be established. In fact, if coevolution takes place, then there should be codependence between landscape and climate properties. The codependence condition, while necessary, is not a sufficient one since it could be merely a statistical coincidence without dynamical grounds.

Whether or not a dynamical mechanism could be present that fairly represented landscape-climate coevolution was addressed by the dynamical model proposed in section 4.2. The model was seen to fairly produce an output consistent with the observed data. In fact, the attractor of the proposed dynamical system as seen by the phase portrait of the pair (Precipitation, Elevation) revealed agreement with the joint distribution of the pair's data.

A rate of coevolution was defined and calculated for Austria and each of its hydroclimatic regions, from the proposed dynamical model and the observed sensitivities, and related to the space-time asymmetry. The nonexistence of coevolution was thus related to space-time symmetry, whereas an increasing coevolution rate would correspond to increased asymmetry between spatial and temporal sensitivity of floods to precipitation.

Rather than dismissing space-for-time substitution, the results have brought to light the need to take into account the different coevolution rates of different regions, associated with different characteristic celerities of the hydrogeological evolution resulting from the heterogeneity of the balances between climate-related forcing and landscape-related resistance. Furthermore, they have stressed the need for a careful assessment of the applicability of the ergodic and Taylor hypothesis prior to engaging in space-for-time trading in geostatistical analysis. On one hand, the interchangeability is found to be legitimate in regions with hydrogeological stability that have had the time to span the whole state space (thus enabling the ergodic hypothesis) or systems that, even not in equilibrium, are evolving at a similar pace (enabling the Taylor hypothesis). On the other hand, regions with transient hydrogeological activity do not comply with such hypothesis, therefore measures of coevolution or relative characteristic celerities have to be taken into account in the space-time trading.

Appendix A: On Information Correlation

We hereby outline the essentials for understanding and computing Information Correlation, used in gauging nonlinear codependence between precipitation and mean catchment elevation in section 3.3. Considering data sets X and Y, Information Correlation is given by *Pires and Perdigão* [2007]:

$$\rho_I(X,Y)=\sqrt{(1-\exp[-2I(X,Y)])} \tag{A1}$$

where

$$I(X,Y)=\sum_{x,y} p_{X,Y}(x,y)\log\frac{p_{X,Y}(x,y)}{p_X(x)p_Y(y)} \tag{A2}$$

is the Mutual Information between X and Y [*Cover and Thomas*, 1991]. The information correlation corresponds to the more traditional Pearson correlation *iff* the joint distribution of (X, Y) is Normal. When the joint distribution is nonnormal, then an inequality between those correlations holds, with the information correlation being higher than the Pearson correlation, as it is able to capture the extra information associated to the nonnormality. As it happens with MI, ρ_I vanishes in the case of statistical independence. In the present context, X and Y represent landscape properties (e.g., mean catchment elevation H) and hydroclimate variables (e.g., mean annual precipitation P). The estimation of Mutual Information and Information Correlation is performed using Maximum Entropy Anamorphoses (MEA), following the theory presented in *Pires and Perdigão* [2012] and the estimators for limited sample sizes from *Pires and Perdigão* [2013]. The MEA method considers, without loss of generality or information, homeomorphisms on the marginals that render them more resistant to outliers and thus more statistically robust.

In order to check whether the Information Correlation measures are significantly different from zero, we apply the Monte Carlo technique in two forms, as in *Pires and Perdigão* [2007]: first, by random series generation (RG), and second by random reordering of working series (RR). The RR method is performed by generating 1000 random series with the same sample size, mean and variance as the original precipitation and flood peak series for each catchment. Then, the correlation measures are recomputed using the generated series. As for the RG procedure, we consider 100 different random permutations within the precipitation and flood peak series for each catchment (shuffling in time), and 100 different permutations of catchment indices for each series (shuffling in space). The correlation measures are then recomputed for the shuffled data. In both approaches (RG and RR), the values of the statistical tests are sorted in such a way as to compute quantiles giving the 95% significance level intervals. As noted in the previous subsection, the statistically significant measures of Information Correlation are flagged with a "*" in Table 5.

Acknowledgment
This research was supported by the ERC Advanced grant "Flood Change," project 291152.

References

Abrahams, A. D. (1972), Environmental constraints on the substitution of space for time in the study of natural channel networks, *Geol. Soc. Am. Bull.*, *83*(5), 1523–1530.

Blöschl, G., M. Sivapalan, T. Wagener, A. Viglione, and H. Savenije (Eds.) (2013), *Runoff Prediction in Ungauged Basins—Synthesis Across Processes, Places and Scales*, 465 pp., Cambridge Univ. Press, Cambridge, U. K.

Champagnac, J.-D., F. Schunegger, K. Norton, F. von Blanckenburg, L. M. Abbhl, and M. Schwab (2009), Erosion-driven uplift of the modern Central Alps, *Tectonophysics*, *474*(1-2), 236–249, doi:10.1016/j.tecto.2009.02.024.

Cover, T. M., and J. A. Thomas (1991), *Elements of Information Theory*, 576 pp., Wiley, N. Y.

Farquharson, F. A. K., J. R. Meigh, and J. V. Sutcliffe (1992), Regional flood frequency analysis in arid and semi-arid areas, *J. Hydrol.*, *138*(3-4), 487–501, doi:10.1016/0022-1694(92)90132-F.

Gaál, L., J. Szolgay, S. Kohnová, J. Parajka, R. Merz, A. Viglione, and G. Blöschl (2012), Flood timescales: Understanding the interplay of climate and catchment processes through comparative hydrology, *Water Resour. Res.*, *48*, W04511, doi:10.1029/2011WR011509.

Gregory, K. J., and D. E. Walling (1973), *Drainage Basin Form and Processes—A Geomorphological Approach*, Edward Arnold, London.

Harman, C. J., P. A. Troch, and M. Sivapalan (2011), Functional model of water balance variability at the catchment scale: 2. Elasticity of fast and slow runoff components to precipitation change in the continental United States, *Water Resour. Res.*, *47*, W02523, doi:10.1029/2010WR009656.

Harvey, A. M. (2002), Effective timescales of coupling within fluvial systems, *Geomorphology*, *44*, 175–201.

Hosking, J. R. M., and J. R. Wallis (1997), *Regional Frequency Analysis: An approach Based on L-Moments*, 224 pp., Cambridge Univ. Press, Cambridge, U. K.

Jefferson, A., G. E. Grant, S. L. Lewis, and S. T. Lancaster (2010), Coevolution of hydrology and topography on a basalt landscape in the Oregon Cascade Range, USA, *Earth Surf. Processes Landforms*, *35*, 803–816, doi:10.1002/esp.1976.

Jenny, H. (1941), *Factors of Soil Formation*, McGraw-Hill, N. Y.

Knox, J. C. (2000), Sensitivity of modern and Holocene floods to climate change, *Quat. Sci. Rev.*, *19*, 439–457.

Kostelecký, V. A., and S. Samuel (1989), Spontaneous breaking of Lorentz symmetry in string theory, *Physica D*, *39*(2), 683–685.

Madsen, M., C. P. Pearson, and D. Rosbjerg (1997), Comparison of annual maximum series and partial duration methods for modelling extreme hydrologic events: 2. Regional modelling, *Water Resour. Res.*, *33*(4), 759–769.

Marsh, W. M., and M. M. Kaufman (2013), *Physical Geography—Great Systems and Global Environments*, Cambridge Univ. Press, N. Y.

Merz, B., S. Vorogushyn, S. Uhlemann, J. Delgado, and Y. Hundecha (2012), More efforts and scientific rigour are needed to attribute trends in flood time series, *Hydrol. Earth Syst. Sci.*, *16*, 1379–1387.

Merz, R., and G. Blöschl (2009), A regional analysis of event runoff coefficients with respect to climate and catchment characteristics in Austria, *Water Resour. Res.*, *45*, W01405, doi:10.1029/2008WR007163.
Merz, R., J. Parajka, and G. Blöschl (2009), Scale effects in conceptual hydrological modeling, *Water Resour. Res.*, *45*, W09405, doi:10.1029/2009WR007872.
Nicolis, C., R. A. P. Perdigao, and S. Vannitsem (2009), Dynamics of prediction errors under the combined effect of initial condition and model errors, *J. Atmos. Sci.*, *66*, 766–778, doi:10.1175/2008JAS2781.1.
Ntegeka, V., and P. Willems (2008), Trends and multidecadal oscillations in rainfall extremes, based on a more than 100-year time series of 10 min rainfall intensities at Uccle, Belgium, *Water Resour. Res.*, *44*, W07402, doi:10.1029/2007WR006471.
Parajka, J., et al. (2010), Seasonal characteristics of flood regimes across the AlpineCarpathian range, *J. Hydrol.*, *394*(12), 78–89, doi:10.1016/j.jhydrol.2010.05.015.
Peel, M. C., and G. Blöschl (2011), Hydrologic modelling in a changing world, *Prog. Phys. Geogr.*, *35*(2), 249–261.
Pickett, S. T. A. (1989), Space-for-time substitution as an alternative to long-term studies, in *Long-Term Studies in Ecology: Approaches and Alternatives*, edited by G. E. Likens, pp. 110–135, Springer, N. Y.
Pires, C. A., and R. A. P. Perdigão (2007), Non-Gaussianity and asymmetry of the winter monthly precipitation estimation from the NAO, *Mon. Weather Rev.*, *135*, 430–448, doi: 10.1175/MWR3407.1.
Pires, C. A. L., and R. A. P. Perdigão (2012), Minimum mutual information and non-Gaussianity through the maximum entropy method: Theory and properties, *Entropy*, *14*(6), 1103–1126, doi:10.3390/e14061103.
Pires, C. A. L., and R. A. P. Perdigão (2013), Minimum mutual information and non-Gaussianity through the maximum entropy method: Estimation from finite samples, *Entropy*, *15*(3), 721–752, doi:10.3390/e15030721.
Prigogine, I., and G. Nicolis (1967), On symmetry breaking instabilities in dissipative systems, *J. Chem. Phys.*, *46*, 3542, doi:10.1063/1.1841255.
Reed, D. W. (1999), *Flood Estimation Handbook*, vol. 1, 108 pp., Inst. of Hydrol., Wallingford, U. K.
Rogger, M., H. Pirkl, A. Viglione, J. Komma, B. Kohl, R. Kirnbauer, R. Merz, and G. Blöschl (2012), Step changes in the flood frequency curve: Process controls, *Water Resour. Res.*, *48*, W05544, doi:10.1029/2011WR011187.
Runyan, C. W., P. DOdorico, and D. Lawrence (2012), Physical and biological feedbacks of deforestation, *Rev. Geophys.*, *50*, RG4006, doi:10.1029/2012RG000394.
Salby, M. L. (1996), *Fundamentals of Atmospheric Physics*, vol. 61, 627 pp., Academic Press, San Diego, Calif.
Salby, M. L. (2012), *Physics of the Atmosphere and Climate*, 666 pp., Cambridge Univ. Press, Cambridge, U. K.
Sivapalan, M., G. Blöschl, R. Merz, and D. Gutknecht (2005), Linking flood frequency to long-term water balance: Incorporating effects of seasonality, *Water Resour. Res.*, *41*, W06012, doi:10.1029/2004WR003439.
Skøien, J., and G. Blöschl (2006), Catchments as space-time filters—A joint spatiotemporal geostatistical analysis of runoff and precipitation, *Hydrol. Earth Syst. Sci.*, *10*, 645–662, doi:10.5194/hess-10-645-2006.
Skøien, J. O., G. Blöschl, and A. W. Western (2003), Characteristic space scales and timescales in hydrology, *Water Resour. Res.*, *39*(10), 1304, doi:10.1029/2002WR001736.
Taylor, G. I. (1938), The Spectrum of Turbulence, *Proc. R. Soc. London, Ser. A*, *164*, 476–490, doi:10.1098/rspa.1938.0032.
Wilks, D. S. (1995), *Statistical Methods in the Atmospheric Sciences—An Introduction*, 467 pp., Academic Press, San Diego, Calif.